J Sol-Gel Sci Technol (2011) 59:158–163
DOI 10.1007/s10971-011-2474-z

ORIGINAL PAPER

Preparation and magnetic properties of $RFeO_3$ nanocrystalline powders

Anhua Wu · Hui Shen · Jun Xu · Linwen Jiang · Liqing Luo · Shujuan Yuan · Shixun Cao · Huaijin Zhang

Received: 2 December 2010 / Accepted: 25 April 2011 / Published online: 7 May 2011

Abstract The rare-earth orthoferrites $RFeO_3$ (R, rare-earth element) crystallize in an orthorhombic distorted perovskite structure. $RFeO_3$ compounds exhibit interesting physical and chemical properties because of their ionic and electronic defects. Polycrystalline nano-sized $RFeO_3$ powders were synthesized by the sol–gel combustion method. X-ray powder diffraction indicated that nanocrystalline powders were single ReFeO3 phase, which are agglomerated with average crystallite size of 60–90 nm estimated with the Scherrer's equation. Magnetic measurements were carried out using a superconducting quantum interference device magnetometer. The influence on hysteresis curve of electronic structure of rare-earth element was investigated for R = Y, La and Nd. Varied magnetic behaviors were observed in these compounds, which are believed to be associated with the different interactions of Fe and rare earths.

Keywords Sol–gel · Combustion · Orthoferrites · Magnetic property

A. Wu (✉) · H. Shen · J. Xu · L. Jiang · L. Luo
Shanghai Institute of Ceramics, Chinese Academy of Sciences, 200050 Shanghai, China
e-mail: wuanhua@mail.sic.ac.cn

S. Yuan · S. Cao
Department of Physics, Shanghai University, 200444 Shanghai, China

H. Shen
School of Materials Science and Engineering, Shanghai Institute of Technology, 200235 Shanghai, China

H. Zhang
State Key Laboratory of Crystal Material, Shandong University, 250100 Jinan, China

1 Introduction

The rare-earth orthoferrites have the general formula $RFeO_3$, where R is a large rare-earth element ion, such as a rare-earth or Y ion. They crystallize in a distorted perovskite structure with an orthorhombic unit cell. The unit cell contains four equivalent iron ions, but the axes of the four surrounding octahedra are slightly tilted with respect to each other. $RFeO_3$ is drawing considerable attention for its applications in various fields, such as fuel cells, catalysts, gas sensors, semiconductors, magnetic materials, and magnetic resonance imaging (MRI) in biomedicine [1–4]. The remarkable properties of orthoferrites, such as high domain-wall velocity and the existence of Bloch lines, have significance for applications in magnetic field sensors and magneto-optical data storage devices [5, 6]. Meanwhile, synthesis of nano-scaled materials is gaining tremendous interest, since ultrafine powder usually exhibits superior properties such as large surface area, higher chemical reactivity, and better sinterability [7].

This family is characterized with interesting magnetic properties. Its weak ferromagnetism was systematically investigated in Ref. [8]. In this work, the influence of 4f electrons of rare earth on the $RFeO_3$ orthoferrites was initially investigated. The outside electron structure of Y^{3+}, Nd^{3+} and La^{3+} is s^2p^6, however La, Nd and Y atoms belong to different groups of transition elements (4f and 3d respectively). As important rare earth ions, La^{3+} has no electrons in 4f, Nd^{3+} has 3 electrons in 4f. Thus, Magnetic measurements were performed on the prepared $YFeO_3$, $LaFeO_3$ and $NdFeO_3$ nanopowder.

Traditional high temperature solid-state reaction has been used to prepare $RFeO_3$, which requires rather high sintering temperature (up to 1600 °C) and suffers from incomplete reaction of the raw materials and easy

formation of undesired phases (i.e., $R_3Fe_5O_{12}$ which is more favored by growth kinetics studies) [9, 10]. Attempts to obtain $RFeO_3$ ultrafine powders have recently been performed by the polyol, sol–gel, heterobimetallic precursor, sonochemical, hydrothermal and combustion methods, etc. [4, 7, 11–14]. Compared with these wet chemical methods, the sol–gel combustion synthesis of $RFeO_3$ exhibits many advantages. The method uses inexpensive precursor, and the experimental process is more simple and easier to operate. The sol–gel combustion method involves a rapid exothermic redox reaction between the metal nitrates and an appropriate fuel, which is ignited at a temperature much lower than the actual phase formation temperature. Therefore, this approach is considered as an attractive method to obtain single phase nanopowder.

In this work, we report the synthesis of nano-crystalline $RFeO_3$ powder by the sol–gel combustion method. In addition, the structure, morphology and magnetic properties of nano-crystalline $RFeO_3$ were also investigated.

2 Experiments

Rare earth oxides R_2O_3 (99.99% purity), $Fe(NO_3)_3 \cdot 9H_2O$(99.99% purity) and citric acid (AR) were used as raw materials. Firstly, the high-purity R_2O_3 and $Fe(NO_3)_3 \cdot 9H_2O$ in the stoichiometric mole ratio of R:Fe = 1:1 were accurately weighted out, respectively. R_2O_3 was dissolved in nitric acid and diluted with distilled water. The concentration of the nitric acid is controlled at about 40–50%. $Fe(NO_3)_3 \cdot 9H_2O$ was also dissolved in distilled water and adequately mixed with the rare earth nitrates. Citric acid was then added as a fuel to the above solution containing R^{3+} and Fe^{3+} to yield a citrate–nitrate ratio of 1.0. After mixing, the final solutions were heated and concentrated by slow evaporation at 85 °C under continuous stirring using a magnetic agitator for several hours. Then the yellowish transparent gels were obtained. Subsequently, the gel was ignited by increasing the temperature up to 250 °C. The dried gel burnt in a self-propagating combustion manner and large volume of brown fume evolved. Finally, a voluminous porous powder was obtained and the powder was calcined at different temperatures in air for 2 h. The experimental procedure is shown as Fig. 1.

Phase identification was checked by powder X-ray diffraction (XRD, D/Max-2550 V, Rigaku, Japan) using Cu Kα radiation and nickel as the filter. The average grain sizes of the powder were estimated following the Scherrer's equation. The magnetic measurements of the samples were performed on a superconducting quantum interference device magnetometer (Quantum design, PPMS-9).

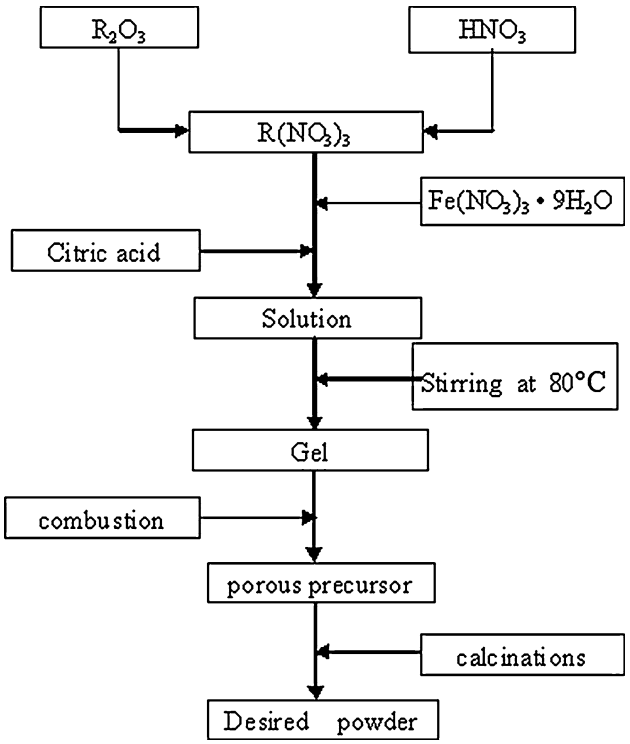

Fig. 1 Flowchart of preparing $RFeO_3$ by the sol–gel combustion method

3 Results and discussion

3.1 Nanocrystalline powders synthesis

The rare-earth orthoferrites $RFeO_3$ nanocrystalline powders, such as $YFeO_3$, $NdFeO_3$, $LaFeO_3$ etc. were successfully synthesized with the sol–gel combustion method [15, 16], XRD measurement indicates that the synthesized powder is single phase of orthoferrite. The XRD patterns of $RFeO_3$ are shown in Fig. 2. The crystallite size of the heat-treated powders was calculated according to the X-ray line-broadening method, using the Scherrer's equation: $D = 0.89\lambda/B\cos\theta$, where D is the crystallite size; λ is the X-ray wavelength (0.15405 nm for Cu Kα); B is the corrected FWHM of the diffraction peak; and θ corresponds to the diffraction angle. The average crystallite size was calculated to be about 30–40 and 60–90 nm for as-burnt powder. The rare-earth orthoferrites $RFeO_3$ nanocrystalline powders can be obtained through calcining at 600–900 °C, the SEM morphology of the $YFeO_3$ powder calcined at 800 °C is shown as Fig. 3.

Generally, the sol–gel combustion often uses fuel, such as citric acid, amino acid, carbamide and hydrazine compound. Amino acid and hydrazine compound is relatively expensive, and the chelate and complex ability of carbamide to metallic cations is weak. Moreover, the combustion temperature of carbamide is up to 1,600 °C, which

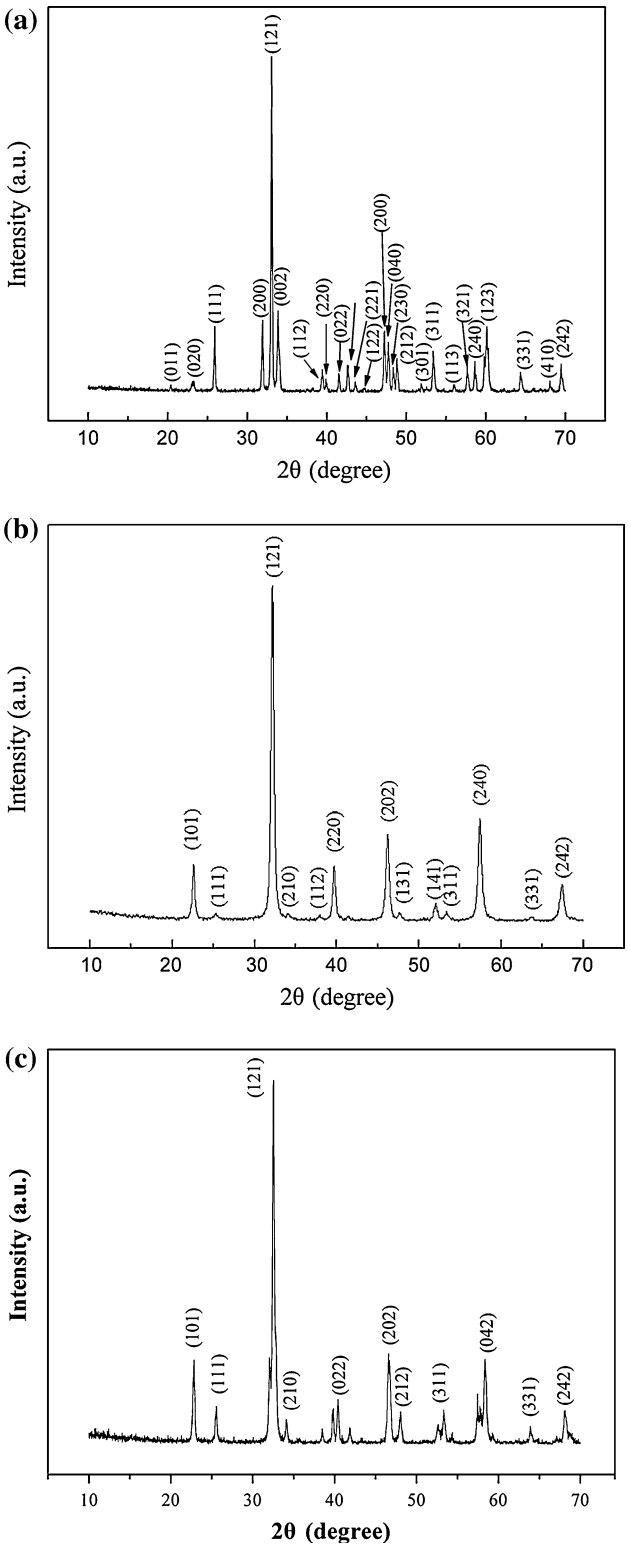

Fig. 2 XRD pattern of $RFeO_3$ nanocrystalline powder. **a** $YFeO_3$. **b** $LaFeO_3$. **c** $NdFeO_3$

is unhelpful to obtain ultrafine powder with good dispersion. Surprisingly, citric acid is a kind of polycarboxylic acid, having low price, strong chelate ability and moderate

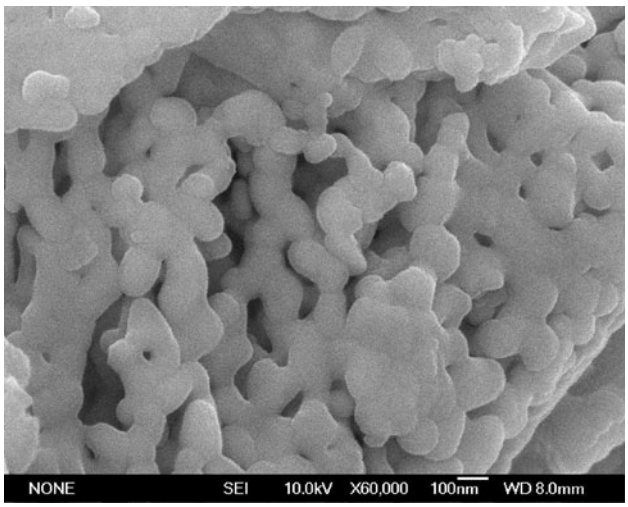

Fig. 3 The SEM morphology of the $YFeO_3$ powder calcined at 800 °C

combustion temperature, which is a good choice as fuel for preparation of $RFeO_3$. The sol–gel is sophisticated technique and requires stringent drying conditions and expensive alkoxide precursors [17]. What is more significant is that the calcination temperature for $RFeO_3$ is rather low by this sol–gel combustion method, since the phase of $RFeO_3$ can be directly formed in the as-burnt powder. Generally, the other methods in related references require calcination temperature up to 800 °C to form the desired $ReFeO_3$ phase.

During the self-propagating combustion process, citric acid acts as the fuel for the combustion process and is oxidized by the nitrates, a large amount of brown fume evolving. The stoichiometric combustion reaction is:

$$3R(NO_3)_3 + 3Fe(NO_3)_3 + 5C_6H_8O_7 = 3RFeO_3 + 30CO_2 + 20H_2O + 9N_2$$

3.2 Magnetic property

The elementary cell of $RFeO_3$ orthoferrites consists of four formulae ABO_3 with atoms distributed in positions such as the ones shown in Fig. 4. The structure can be visualized as a three-dimensional network of strings of FeO_6 octahedra. The orthoferrite $RFeO_3$ crystallizes in a distorted perovskite structure with an orthorhombic unit cell. The distortion from the ideal cubic perovskite is mainly in the position of the R ions, where the Fe^{3+} ions are present in an essentially octahedral environment. In orthoferrite $RFeO_3$, the six-coordinated iron octahedra have been slightly tilted, lowering the symmetry to orthorhombic. The magnetic moments of iron and rare earth atoms as well as the interactions between them are the source of the magnetic properties of these orthoferrites. Rare earth and iron atoms

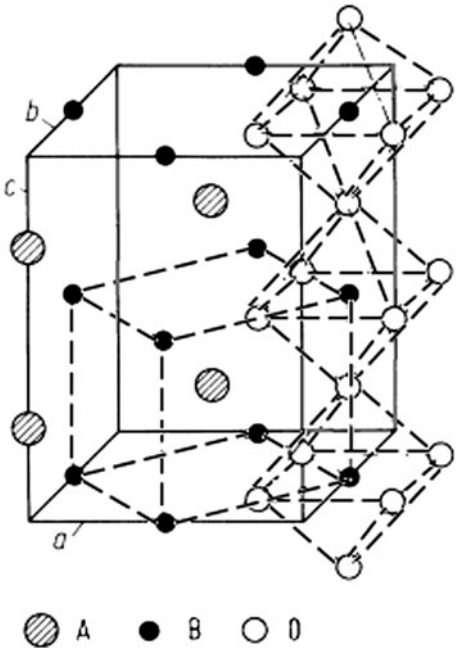

Fig. 4 ABO_3 Orthorhombic distortion of crystal structure

belong to different groups of transition elements (4f and 3d respectively) with different magnetic moment values. It is common to divide all the interactions into the R–R, the Fe–Fe and the Fe–R ones, each one generally consisting of isotropic, antisymmetric and anisotropic symmetric super-exchanges. A well-known feature of orthoferrites is the strong anisotropy of various origins, which depends essentially on the rare-earth atoms of compounds. The antisymmetric component of the super-exchange interaction manifests itself as the non-colinear magnetic structures of various types which are characteristic for this family of compounds. The room-temperature magnetic hystereses of these compounds ($YFeO_3$, $LaFeO_3$ and $NdFeO_3$) are shown in Fig. 5.

The magnetization versus magnetic field (M–H) curve of $YFeO_3$ nanopowder displays obvious rectangular hysteretic loop, and the saturation magnetization (M_s) reaches 0.15 emu/g and coercive field H_c is about 40 kOe. Although the $RFeO_3$ orthoferrites are canted antiferromagnets, $YFeO_3$ exhibits ferromagnetic behavior, which maybe due to special outside ionic structure of Y^{3+} ($3d^0$). In $LaFeO_3$ nanopowder, there is a hysteresis loop at room temperature with a spontaneous magnetization. The shape of the hysteresis loop is also characteristic of weak ferromagnetism. However, even a field of 20 kOe does not saturate the magnetization curve, and the magnetization still has a tendency to increase, which is characteristic of the mainly anti-ferromagnetic ordering of the spins in the nanoparticles. The coercive field is about 137 Oe and the spontaneous magnetization is about 0.10 emu/g. The spontaneous magnetization is directly estimated by extrapolating the linear part of M(H) to H = 0 Oe [18]. The M–H curve of $NdFeO_3$ nanopowder is also shown in Fig. 5, the maximum field applied is 20 kOe, too. Different from $YFeO_3$ and $LaFeO_3$, the shape of the hysteresis loop of $NdFeO_3$ nanopowder exhibits typical characteristic of anti-ferromagnetism, the magnetization still has an identical tendency to increase even at a field of 20 kOe.

In addition, the saturation magnetization (M_s) of $RFeO_3$ is no more than 0.30 emu/g in this work. It is obviously lower than those in the earlier references [19–21], in which the saturation magnetization of $YFeO_3$, $LaFeO_3$ and $NdFeO_3$ are all more than 1 emu/g. However, the coercivity of $RFeO_3$ in this work is similar with those in the earlier references. It maybe originated from the nanosized effect of $RFeO_3$ powder because the average sizes in earlier references are all more than 200 nm. Nanocrystalline $RFeO_3$ exhibits high coercivity and low saturation magnetization in reference [20].

The $RFeO_3$ family shows various interesting magnetic coupling, due to different 4f electrons distribution of rare earth element and the interaction between Fe ions and rare earth element. Generally, the magnetic moments of iron and rare earth atoms as well as the interactions between them are the source of the magnetic properties of $RFeO_3$. The magnetic superexchange interactions between the Fe ions result in collinear anti-ferromagnetic spin order which contributes to the anti-ferromagntic coupling along a particular crystallographic direction. However, low symmetry of the distorted orthorhombic perovskite-type structure leads to the tilt of FeO_6 octahedra. Consequently, a canted spin order is also formed in the Fe lattice, which gives rise to weak ferromagnetism along another crystallographic direction [22, 23]. The FeO_6 octahedra can be tilted to different degree depending on the size of the rare-earth cation, leading to different net magnetic moment [24].

As discussed above, typical ferromagnetic coupling is observed in $YFeO_3$. However, the coercivity and remnant magnetization are small for $LaFeO_3$ and $NdFeO_3$. So their magnetic behaviors were investigated in more detail. The magnetization versus temperature M (T) in 100 Oe field with zero-field-cooled (ZFC) and field-cooled (FC) modes for $LaFeO_3$ and $NdFeO_3$ are shown in Fig. 6. $NdFeO_3$ has two magnetic sublattices, and the Fe sublattice is antiferromagnetism, while the magnetic moments of Nd ions have negative temperature coefficient. Below 35 K, the magnitude of Nd moments is larger than that of Fe cations, and ferromagnetic-like situation which is revealed by ZFC curve as shown in Fig. 6a may occur. However, moments of Nd decreases with the increasing temperature, which induces the drop in magnetization up to 35 K. Thereafter, the antiferromagnetism of Fe sublattice becomes prominent

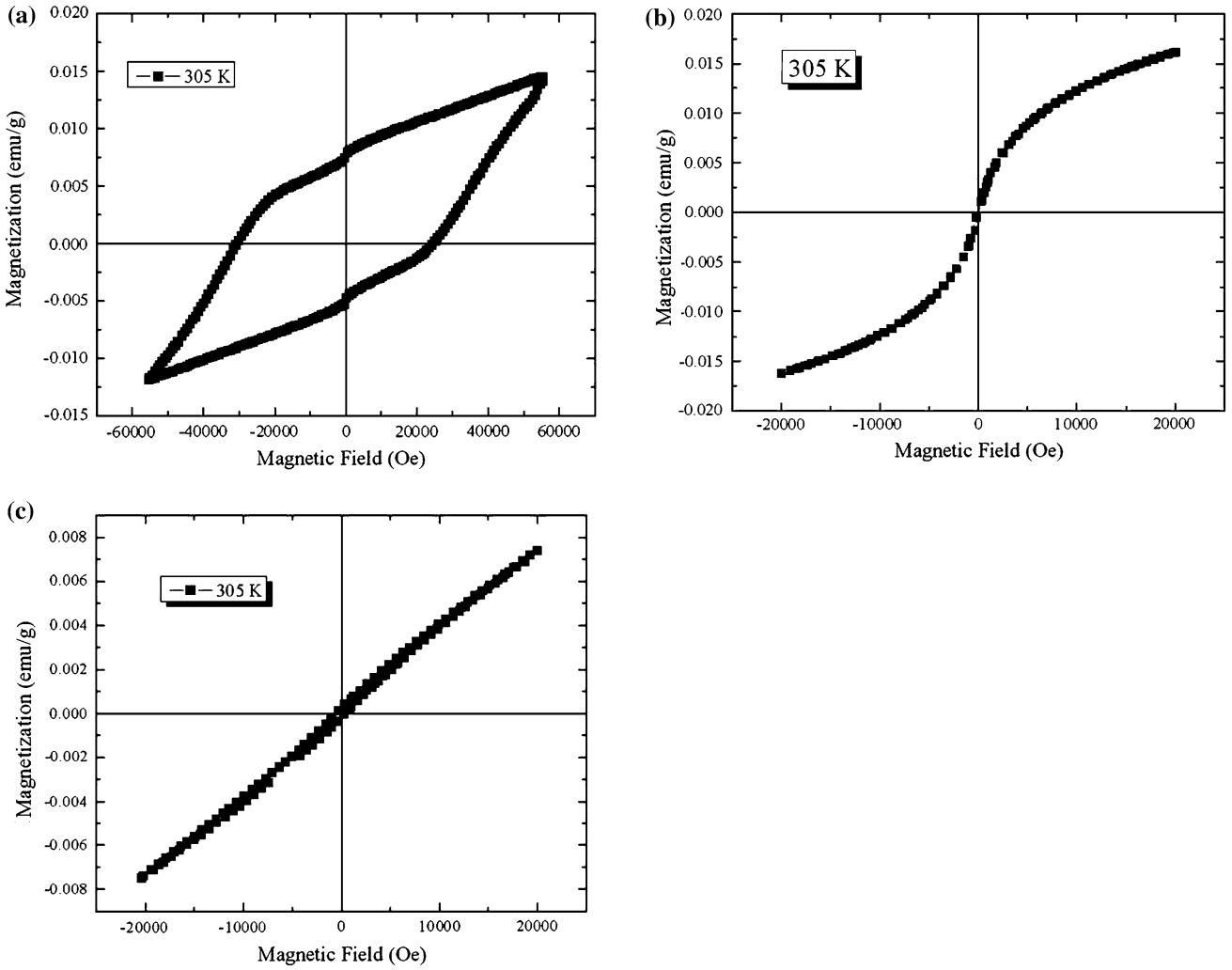

Fig. 5 Room temperature hysteresis curve of $YFeO_3$, $LaFeO_3$ and $NdFeO_3$. **a** $YFeO_3$. **b** $LaFeO_3$. **c** $NdFeO_3$

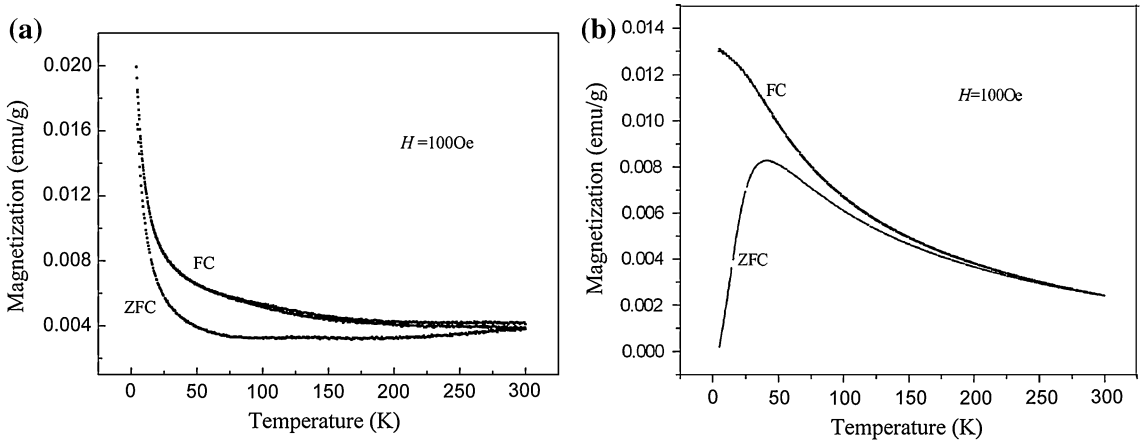

Fig. 6 Temperature dependence of the magnetization after ZFC and FC measured at 100 Oe. **a** $NdFeO_3$. **b** $LaFeO_3$

[25]. The behavior of $LaFeO_3$ is different from that $NdFeO_3$. The magnetization in FC curve decreases continuously with increasing temperature, and a cusp in the ZFC curve is observed around 38 K. These characteristics are interpreted as the evidence of magnetic frustration or glassy behavior [26].

4 Conclusions

The polycrystalline nano-sized $RFeO_3$ powders were synthesized by the gel combustion method, and the average crystallite size is 60–90 nm. Nanocrystalline $RFeO_3$ exhibits high coercivity and low saturation magnetization due to the nanosized effect. As anti-ferromagntic materials, some $RFeO_3$ orthoferrites exhibit weak ferromagnetism due to the empty of 4f electrons. Maybe the empty of 4f electrons in R^{3+} ions is also a main reason of anti-ferromagnetism in $RFeO_3$ orthoferrites exhibiting weak ferromagnetism, which needs further investigation and research in the future.

Acknowledgments The authors would like to acknowledge the financial support from National Natural Science Foundations of China (Grant No. 50932003 and 51002097). This work is also supported by the Opening Project of State Key laboratory of Crystal Material (Grant No. KF1006).

References

1. Minh NQ (1993) J Am Ceram Soc 76:563
2. Niu XS, Du WM, Du WP (2004) Sens Actuators B 99:399
3. Fredrik S, Marc AF, Rodrigo PJ, Anna K, Teodor V, Maria E, Kajsa U, Per-Olov K (2008) Nanotechnology 19:085608
4. Delmastro A, Mazza D, Ronchetti S, Vallino M, Spinicci R, Brovetto P, Salis M (2001) Mater Sci Eng B 79:140
5. Ripka P, Vertesy G (2000) J Magn Magn Mater 215:795
6. Didosyan YS, Hauser H, Reider GA, Toriser W (2004) J Appl Phys 95:7339
7. Mathur S, Shen H, Lecerf N, Kjekshus A, Fjellvag H, Goya GF (2002) Adv Mater 14:1405
8. Bombik A, Lesniewska B, Pacyna AW (2000) J Magn Magn Mater 214:243
9. Ravindranathan P, Komarneni S, Roy R (1993) J Mater Sci Lett 12:369
10. Buscaglia V, Caracciolo F, Bottino C, Leoni M, Nanni P (1997) Acta Mater 451:213
11. Qi X, Zhou J, Yue Z, Gui Z, Li L (2003) Ceram Int 29:347
12. Zheng W, Liu R, Peng D, Meng G (2000) Mater Lett 43:19
13. Sivakumar M, Gedanken A, Bhattacharya D, Brukental Y, Yeshurun Y, Zhong W, Du Y, Felner I, Nowik I (2004) Chem Mater 16:3623
14. Rajendran M, Bhattacharya AK (2006) J Eur Ceram Soc 26:3675
15. Shen H, Cheng G, Wu A, Xu J, Zhao J (2009) Phys Stat Sol (a) 206:1420
16. Wu A, Cheng G, Shen H, Xu J, Chu Y, Ge Z (2009) Asia-Pac J Chem Eng 4:518
17. Vajargah SH, Hosseini HRM, Nemati ZA (2007) J Alloys Compd 339:430
18. Bozorth RM, Williams HJ, Walsh DE (1956) Phys Rev 103:572
19. Mathur S, Veith M, Rapalaviciute R, Shen H, Goya GF, Filho WL, Berquo TS (2004) Chem Mater 16:3623
20. Qi X, Zhou J, Yue Z, Gui Z, Li L (2002) Mater Chem Phys 78:25
21. Slawinski W, Przenioslo R, Sosnowska I, Suard E (2005) J Phys Condens Matter 174:605
22. Parida SC, Rakshit SK, Singh Z (2008) J. Solid State Chem 181:101
23. Mathur S, Veith M, Rapalaviciute R, Shen H, Goya GF, Filho WL, Berquo TS (2004) Chem Mater 16:1906
24. Cristobal AA, Botta PM, Bercoff PG (2009) Mater Res Bull 44:1036
25. Zhang Y, Zhang H, Yin J, Zhang H, Chen J, Wang W, Wu G (2010) J Magn Magn Mater 322:2251
26. Mao J, Sui Y, Wang X, Yang Y, Zhang X, Wang Y, Wang Y, Liu W (2008) J Alloy Compd 509:4950